Elucidating the Membrane Binding Process of the LKB1 C-terminus via Atomistic Simulations: Dynamic Interplay of Anionic Lipids and the Polybasic Region

Azadeh Alavizargar[1*], Maximilian Gass[2], Michael P. Krahn[2], Andreas Heuer[1],

1 Institute of Physical Chemistry, University of Münster, Corrensstr. 28/30, 48149 Münster, Germany
2 Medical Cell Biology, Medical Clinic D, University Hospital of Münster, Albert-Schweitzer Campus 1-A14, 48149 Münster, Germany

* aalaviza@uni-muenster.de

Abstract

Liver kinase LKB1 is a serine/threonine kinase, which functions as a master kinase, activating several downstream kinases. Thereby, it is implicated in many cellular processes such as cell proliferation and cell polarity. Moreover, LKB1 regulates cell cycle progression and apoptosis and is mutated or downregulated in various types of cancer. LKB1 itself becomes fully activated upon recruitment to the plasma membrane by binding of its C-terminal polybasic motif consisting of eight Lysines/Arginines to phospholipids. Here we present extensive molecular dynamics (MD) simulations of the C-terminus of LKB1 containing the polybasic motif interacting with a model membrane composed of phosphatidylcholin (POPC) and phosphatidic acid (PA).
Protein-membrane binding effects are due to the electrostatic interactions between the polybasic amino acids and PA lipids. For significant binding the first three lysines turn out to be dispensable, which was also recapitulated in cell culture using transfected GFP-LKB1 variants. LKB1-membrane binding results in a structural change of the protein as well as of the membrane, in particular accumulation of PA lipids and reduced thickness at the protein-membrane contact area. The protein-lipid binding turns out to be highly dynamic due to an interplay of PA-PA repulsion and protein-PA attraction. The thermodynamics of this interplay is captured by a statistical fluctuation model, which allows the estimation of both energies. Quantification of the significance of each polar amino acid in the polybasic provides detailed insights into the molecular mechanism of the protein-membrane binding of LKB1. The results likely can be transferred to other proteins, which interact by intrinsically disordered polybasic regions with anionic membranes.

Author summary

The interaction of disordered regions of proteins with membranes, particularly when containing anionic lipids, is of significance for their functionally. In this work we show the mechanism of the binding of the C-terminus of the LKB1 protein, which has a disordered structure and contains a poly-basic region, with the membranes containing phosphatidic acid (PA). We show how the structure and dynamics of the protein and the dynamics and the lateral distribution of PA are modified as a result of the interaction. The protein-lipid binding was found to be highly dynamic. Via

thermodynamic modelling of the fluctuations, we can estimate the PA-PA repulsion and protein-PA attraction energies. We additionally show which amino acids are critical for the binding by testing two levels of mutation in the poly-basic region. We believe that our results shed light on the general mechanism of the interaction of disordered proteins with anionic membranes, revealing the mechanism of the protein-membrane binding process and the nature of the lateral fluctuations of the acidic lipids.

Introduction

Liver kinase B1 (LKB1) is a highly conserved serine/threonine kinase, which functions as a tumor suppressor and has been proposed as a 'master kinase', activating several downstream kinases in particular of the AMPK-family [1]. This kinase is also involved in various cellular signalling pathways, including Wnt-, TGFb-signalling or the mTOR-pathway [2]. Apart from its function in cell proliferation and tumour suppression, LKB1 plays an important role in the establishment and maintenance of cell polarity in different cell types [3].

The localization and activity of LKB1 is controlled by two pseudokinases: STRAD (Ste20–like kinase (Stlk) in Drosophila) and Mo25 [4]. These proteins facilitate the export of LKB1 from the nucleus to the cytoplasm [4, 5]. Subsequently, LKB1 is localized to the plasma membrane (PM) by a C-terminal phospholipid binding domain and its farnesylation motif. The farnesylation has been, however, reported not to be essential for the tumour suppression function of LKB1 in cultured mammalian cells or mice and Drosophila in vivo, [6–8]. In contrast, the polybasic motif adjacent to the farnesylation motif is crucial for stable membrane recruitment and fully activation of the kinase activity of LKB1 [8].

Membrane association of proteins can be accomplished by direct binding, e.g. by distinct lipid-binding domains. Apart from larger domains, polybasic motifs in several proteins have been shown to bind to various phospholipids [9–13]. For LKB1, it has been reported that the C-terminal polybasic region (aa 539–551), which includes eight charged amino acids(lysines and arginines (Ks,Rs)), facilitates a direct binding to PA and to much less extent to PtdIns(3,4,5)P3 and PtdIns(4,5)P2 lipids [8]. The mutation of these residues to alanine has been shown to abolish the protein-membrane binding in vitro as well as in cultured cells and in Drosophila in vivo [8]. The amino acid sequences for the wild-type (WT) and the mutated (MT) proteins with highlighted polar (in cyan) and mutated (in red) residues are shown in Table 1. However, cell biological studies leave important questions unanswered, in particular, how exactly the binding of distinct amino acids within the polybasic motif reinforces binding of the entire protein to the membrane, how dynamic the protein-lipid binding is, and whether binding of LKB1 induces a local clustering of PA in microdomains, which in turn strengthens binding of the polybasic motif to the membrane. Furthermore, despite the considerable progress in computational resources and force fields, the protein-lipid interaction studies remain at the qualitative level. Concerning atomistic simulations, apart from the accuracy of the force fields, there is a challenge of conformational sampling, especially for intrinsically disordered proteins (IDPs). This is even more challenging in the case of the interaction of IDPs with anionic membranes.

Therefore, in this work we probe the significance of PA lipids as well as single amino acids within the polybasic region of LKB1 for the membrane-binding. For this purpose, we study the unstructured C-terminal region of the Drosophila LKB1 protein as well as its mutants with membranes containing various amounts of PA, using extensive microsecond scale molecular dynamics (MD) simulations, alleviating the issue of conformation sampling. The simulations are complemented by experiments in transfected cells with GFP-tagged variants of LKB1, comparing the protein-membrane

Table 1. Sequences of the WT and MT proteins. The polar (cyan) and mutated (red) residues are highlighted.

protein	sequence
WT	^{536}APVKKKGSALKRRAKKLTS^{554}
3KMT	^{536}APVAAAGSALKRRAKKLTS^{554}
MT	^{536}APVAAAGSALAAAAAALTS^{554}

binding of the wild type with different mutations. Our systematic analysis shows the significance of PA lipids for the protein-membrane binding and the effect of partial mutation of the polybasic region. Using the spatio-temporal resolution of MD simulations, we specifically show how the structure of the protein is affected as a result of the interaction with the membrane during the binding process and the stationary state at long time scale. We also show how the lateral distribution of PA molecules is affected by the presence of the interacting protein. These results shed light on the mechanism of the protein-membrane interaction of LKB1 and the family of proteins interacting with membranes via polybasic regions, and in general, the interaction of IDPs membranes including anionic lipids.

Materials and methods

System setup

For all simulations, we took a protein of 19aa from aa 536-554 of Drosophila LKB1 containing the polybasic motif in the C-terminus of the LKB1 protein [8]. The initial atomistic 3D structure of this protein segment was constructed using the SWISS-MODEL homology modeling web server. [14–16]. Accordingly, the model was built based on the 50S ribosomal protein L32 (PDB:1OND), with a sequence similarity of 37% and a sequence coverage of 66%. Note that the structure is supposed to be a disordered protein. Then CHARMM-GUI solution and membrane builder [17] was used to prepare the systems with solvated proteins or the systems including also a membrane. During the process of the modeling, the protein is amidated and acetylated and finally solvated by water molecules with the addition of neutralizing ions, depending on the membrane composition and amount of the charge in the system. Concerning the salt concentration, we should mention that the binding of monovalent ions to the lipid headgroups is especially problematic and their binding affinity is not captured correctly by any of the PS force fields and their interaction with membrane is overestimated [18, 19]; therefore, we decided to only use the neutralizing ions. In the next step, the WT protein was simulated in solution in a few independent simulations for 200 ns. Then the structures at the end of these simulations were extracted and used to be combined with membranes of different compositions using CHARMM-GUI membrane builder [17]. The total number of lipids in the simulated systems is around 200. Additionally, two mutated models of the protein were constructed during the process of combining it with membrane: 1) the first three lysine residues are mutated to alanine (3KMT) and 2) all the lysine and arginine residues are mutated to alanine (MT). The amino acid sequences of the WT and the MT proteins are indicated in Table 1 and the simulated systems, including the lipid composition, number of samples and the simulation time for each sample are represented in Table 2.

Table 2. Simulation systems along with the protein type and membrane compositions as well as the number of samples and the simulation time are shown.

system	protein	membrane	No. of PAs	sample	sim time [μs]
WT-0%PA	WT	POPC100%	0	7	2
WT-5%PA	WT	POPC95%-POPS5%	10	10	2
WT-10%PA	WT	POPC90%-POPS10%	20	13	2
WT-20%PA	WT	POPC80%-POPS20%	40	7	2
3KMT-0%PA	3KMT	POPC100%	0	5	0.15
3KMT-10%PA	3KMT	POPC90%-POPS10%	20	5	2
MT-10%PA	MT	POPC90%-POPS10%	20	7	2-4

0.1 Simulation protocol

The MD simulations were performed using Gromacs version 2019.6 [20, 21]. The CHARMM36m force field [22, 23], which is a modified version of the CHARMM36 force filed for IDPs, and the TIP3P water model [24] were used to define the interactions. Periodic boundary conditions were applied in all directions. The long-range electrostatic interactions were considered using the particle mesh Ewald method [25], using the cutoff distance of 1.2 nm and the compressibility of 4.5×10^{-5}. To treat van der Waals (vdW) interactions, the cut-off schemes with the cutoff distance of 1.2 nm were used, which is smoothly truncated between 1.0 and 1.2 nm. The electrostatic interactions were considered using the particle mesh Ewald method [25]. The constant pressure for the protein-membrane systems was semi-isotropically maintained at 1 bar with the use of Berendsen [26] and Parinello-Rahman barostats [27], respectively for the equilibration and the production simulations. The constant temperature at 310 K was controlled by coupling the system to the Nosé-Hoover thermostat [28, 29]. The bonds were constrained using the LINCS algorithm [30]. Before the equilibration process, all systems were first minimized in 10000 steps. The protein-membrane systems were subsequently equilibrated using initially the NVT (2ns) and then the NPT (28 ns) according to the input files provided by CHARMM-GUI. During the course of equilibration, restraints (starting with 4000 kJ/mol^{-1}.nm^{-2}) were applied on the heavy atoms of the protein and the lipids, which were in multiple step gradually decreased to 50 kJ/mol^{-1}.nm^{-2}. The production simulations were performed for 2 μs using a time step of 2 fs. For the MT system the simulation were continued for 4 μs. In order to provide statistically independent simulations, for each system different samples were run using different structures of the protein extracted from the simulations of the protein in a solution without the presence of membrane. For these simulations, the same protocol was used as the protein-membrane systems except that the isotropic pressure coupling was utilized and for each simulation the production simulations were performed for 200 ns.

The simulation results were analyzed using in-house python codes, incorporating the MDAnalysis package [31, 32] and the GROMACS tools. VMD was employed to visualize the trajectories and prepare the snapshots [33]

0.2 Order parameter

The order parameter of the lipid chains was calculated according to ref. [34], using molecular order parameter formula defined as

$$S = \frac{1}{2}\left\langle 3\cos^2\Theta_n - 1\right\rangle \tag{1}$$

where Θ_n is the angle between the vector constructed by nth segment of the hydrocarbon chain, i.e. C_{n-1} and C_{n+1}, connecting the $n-1$ and $n+1$ carbon atoms,

and the membrane normal (z-axis). The angular brackets represent the time and ensemble average.

0.3 Cell culture and transfection

Schneider S2R+ cells on coverslips were transfected with GFP-LKB1 variants under a ubiquitous promoter (Ubi::GFP-LKB1) using FUGENE (Promega) [35]. 48 h after transfection, cells were fixed with 4% paraformaldehyde in PBS pH7.4 for 20min. Subsequently, cells were washed three times with PBS and nuclei were labelled with DAPI for 20min. Cells were mounted in Mowiol and imaged with a confocal microscopy (Leica SP8).

Results

1 Results: Protein perspective

1.1 PA is essential for the protein-membrane binding of LKB1

In all systems the protein is first in solution at the beginning of the simulations, so that the distance of the center of mass (COM) of the protein from the center of the membrane along the membrane is 6 nm (Fig 1A top) and the protein can freely move. Depending on the membrane composition, the protein can be attracted to the membrane and interact with it (Fig 1A middle,bottom). In order to check if the protein interacts with the membrane we plotted the projected distance of the COM of the protein and the closest heavy atom of the protein from the center of the membrane along the membrane normal (z-axis) (Fig 1B-F). For membranes without PA lipids (WT-0%PA system , Fig 1B), the protein can occasionally approach the membrane and interact with it, but no persistent protein-membrane binding takes place. However, as soon as 5% PA lipids (or more) is added to the membrane persistent interactions of the protein with the membrane occur (Fig 1C). Thus, a small fraction of PA lipids is sufficient for a stable protein-membrane binding.

Interestingly, the mutation of the first three lysine residues to alanine (3KMT-10%PA) does not abolish the stable interaction with the membrane (Fig 1D). Conversely, when all the lysine and arginine residues are mutated to alanine (MT-10%PA), either no interaction with the membrane takes place (Fig 1E) or only short binding periods (Fig 1F).

In order to confirm that our simulations represent the behaviour of the protein in vivo, we transfected cells with GFP-tagged variants of LKB1. Indeed, while wild type full length LKB1 or a truncation of LKB1 containing the last 49aa (LKB1 518-C) accumulates mainly at the plasma membrane, mutation of all positively charged amino acids (LKB1LB = lipid-binding) abolishes membrane binding resulting in a cytoplasmic accumulation of the mutant protein (Fig 22A, B, D). Strikingly, as predicted from our simulations, mutation of the first three lysines (3KMT) did not substantially affect cortical localization of LKB1 (Fig 2C).

1.2 Protein's embedding in membrane

The general protein-membrane interaction is also reflected in the density plots of the protein and lipids (Fig 1G), showing to what extent the protein can be attracted to the membrane. The density plots show that the protein with the higher amount of PA lipids in the membrane can systematically penetrate the membrane more efficiently. Interestingly, for the 3KMT-10%PA system, the protein can approach the membrane

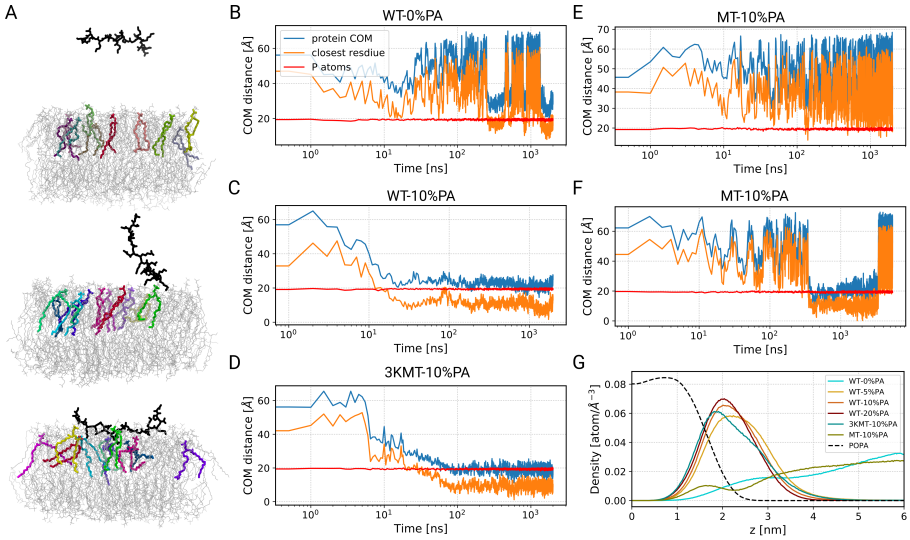

Fig 1. Presence of PA and mutation of the polybasic region affect the protein-membrane binding. A) The snapshots of the protein-membrane system for the WT-10%PA system at different times of the simulation are shown. The protein and PAs in one leaflet are shown respectively in black and colored licorice representation. The PC lipids are shown as grey lines. B-F) The distance of the COM of the protein with respect to the center of the membrane (blue), the closest heavy atom of the protein (orange) and the average position of the P atoms of the lipids (red) projected on the membrane normal (z-axis) as a function of time for different systems are shown. E and F correspond to two different realizations. G) The density of the protein in different systems as well as the density of PA lipids (dashed line) are represented.

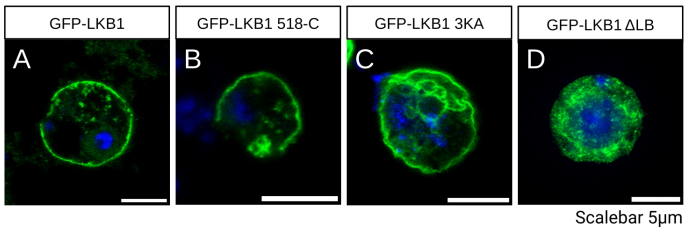

Fig 2. Mutation of the lipid-binding motif results in disturbed membrane association of LKB1. A-D) Schneider 2R+ (S2R+) cells were transfected with GFP-LKB1 variants and stained with DAPI. Wild type LKB1 (A) and the isolated C-terminus (amino acids 518-566, B) accumulate predominately at the plasma membrane, whereas mutations of all basic amino acids results in cytoplasmic aggregates (D). LKB1 with a mutation of only three basic amino acids within the polybasic motif is still robustly targeted to the cortex (C).

stronger than the WT one (WT-10%PA), while some parts of it remain further separated from the membrane due to the mutation. As expected, both MT-10%PA as well as WT-0%PA display even repulsive interaction with the membrane. The observation from Fig 1F about the temporary binding of the 3KMT-10%PA system is reflected by the small maximum around 1.5 nm.

1.3 Protein's structural changes

Next we looked at how the structural properties of the protein is affected as a result of the interaction with the membrane. The root-mean-squared deviation (RMSD) in steps of 50 ns for the WT-10%PA system (S1 FigA) and the average of RMSD values for all systems (S1 FigB) are shown. The RMSD for WT systems dramatically decreases for pure membrane system and only slightly decreases for the WT systems with increasing amount of PA. The 3KMT-10%PA system shows the highest RMSD value, which is due to the presence of the weakly bound mutant part of the polybasic motif that causes the protein to be highly flexible.

Since the protein does not have a well-defined secondary structure, its structure dramatically changes as a result of the protein-membrane interaction. Therefore, we analysed these structural changes in more detail: The average of the sum of squared distances of CA atoms of the protein amino acids from the COM of the protein backbone, once projected along the z-axis (Δz) and once on the xy-plane (Δr), i.e. the respective standard deviations was calculated. These values were then normalized by the corresponding values for the free proteins inside the solution in the systems without PAs (WT-0%PA and 3KMT-0%PA), which do not interact with the membrane (Δz_{norm} and Δr_{norm}). Therefore, a value of unity represents a property close to that of the free protein in solution without the interaction with the membrane. As the protein binds to the membrane, Δz_{norm} gradually reduces and adopts values below 1. This reflects a generic behavior that along with the binding processes of amino acids with the membrane a flattening of the protein takes place. Interestingly, in the long-time range the normalized standard deviation increases again (Fig 3A). A slightly different behaviour is observed for the 3KMT-10%PA system. Here the time-averaged normalized standard deviation is close to unity. This may be related to the fact that the mutations reduce the strength of the interaction with the membrane. Along with this interpretation the reduction in the standard deviation Δz is most pronounced for systems with a higher concentration of PAs (Fig 3A right).

For all systems except for WT-5%PA the value of Δr_{norm} conversely increases as a result of the interaction for intermediate times and for longer times approaches the value, seen for the non-interacting case (Fig 3B). To a good approximation this behaviour is opposite to the time dependence of Δz_{norm}. This stretching increases the free energy of the protein and is likely counterbalanced by the enthalpic interaction with the membrane in particular with PA. The disappearance of this stretching effect for long time periods (Fig 3B right) suggests that some reorganization of the PA distribution occurs, which we will address further below. The opposite trend for the time-dependence for WT-5%PA may be related to the lower number of PAs.

Next, we analyze $\Delta r^2 \Delta z$, reflecting the effective volume of the protein (Fig 3C). While the time-dependence is somewhat difficult to interpret, we clearly see that for the WT the final volume is quite insensitive to the PA content. However, as compared to the WT without significant binding effects, i.e. with no PA, the volume shrinks by approx. 25%. The different volume for 3KMT-10%PA reflects the different sequence of this protein.

Finally, in Fig 3D we show the time-dependence of the conformation for the representative example of WT-10%PA. While for short times no direction is preferred, for intermediate times one can see that the protein adopts the shape of an oblate spheriod. This is compatible with the increase of Δr^2 and the decrease of Δz . In the equilibrated states the shape becomes somewhat more spherical but with a smaller volume compared to the initial unbound state.

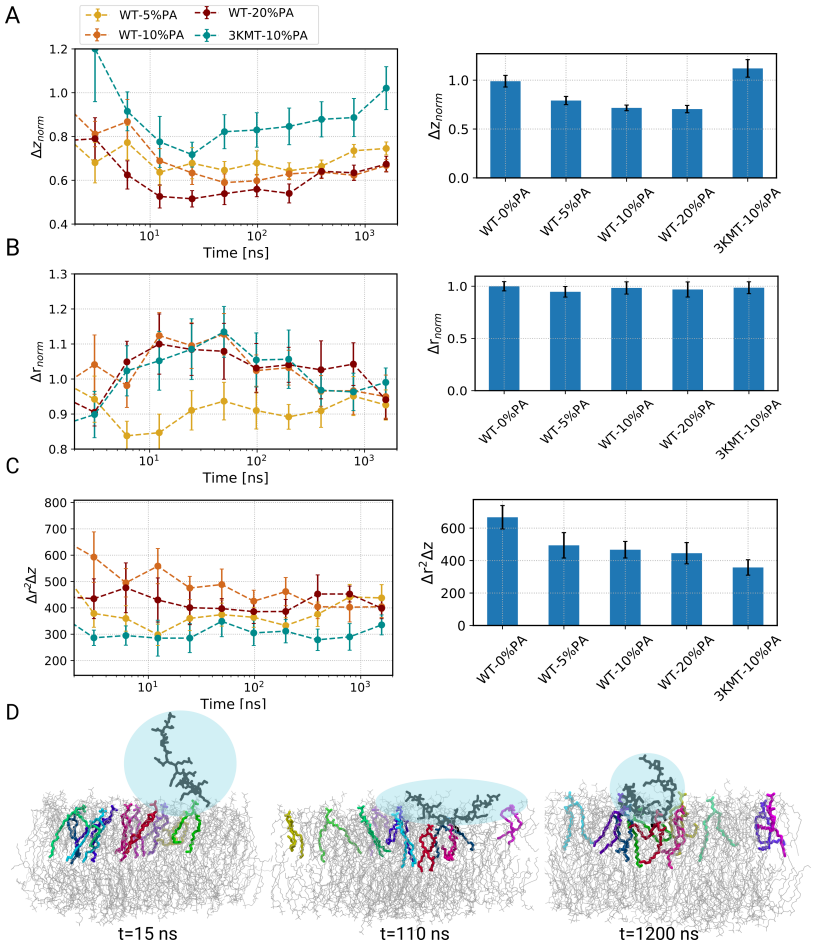

Fig 3. Structural properties of the protein changes during the course of membrane binding. A) The root mean squared of the average distances of CA atoms of the protein from the COM of the backbone atoms of the protein projected on the z-axis (Δz_{norm}) and B) the xy-plane (Δr_{norm}). C) The volume of the protein, defined as $\Delta r^2 \Delta z$, i.e., without any normalization, are shown over blocks of the simulation time. The corresponding average values of the quantities in A-C for the last 500 ns of the trajectory are represented in bar plots. D) The snapshots of the protein on the membrane, showing various representative structures, at different times of the simulation for the WT-10%PA. The protein is shown in black and the PAs in the interacting leaflet in different colors, using licorice representation.

2 Results: Protein - PA interplay

2.1 The polybasic motif of LKB1 mainly binds to PAs

The structural changes in the protein structure, discussed in the previous section, indicate the presence of a subtle interplay of protein conformation and PA arrangement. Therefore, in this section we analyzed the protein-membrane interaction in more detail, starting with the percentage of lipids interacting with the protein throughout the simulations. The number of interacting lipids was based on the number of contacts using a cut-off distance of 4.0 $\mathring{A}$ between any atoms of the protein and the lipids headgroup. The results show that the protein binds to the membrane in the first few nanoseconds. Interestingly, when the amount of PA is lower than or equal to 10%, the number of

lipids reaches a final value quite fast (Fig 4A,B), whereas in the case of WT-20%PA, it takes a comparatively long time until an optimum interaction state is achieved (Fig 4C).

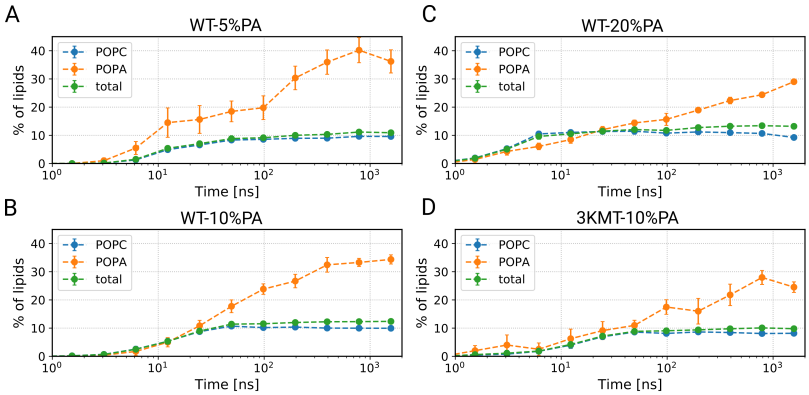

Fig 4. Time evolution of the percentage of interacting PA with the protein. A-D) The average of the percentage of different lipid types interacting with the protein for different systems is shown.

If there were well-defined binding sites for PAs within the polybasic motif , one would expect that the absolute number of PA molecules close to the protein should be insensitive to the PA concentration. Then the fraction of bound PAs would correspondingly decrease for increasing PA concentration. However, we see that there is only a very small decrease of the fraction of bound PA (approx. 35% for WT-5%PA and slightly smaller values for WT-10%PA and WT-20%PA). This implies a strong increase of the absolute number of PAs with increasing PA concentration. As a consequence, the attraction of the PAs may take longer for higher PA content. As expected, the 3KMT protein is not able to interact with the same number of lipids as in the WT system due to the point mutations (Fig 4D).

To explore the translocation process in more detail, we calculated the 2-dimensional mean-squared displacement (MSD) of the protein and PAs in different systems along the membrane plane for the last 500 ns of the simulations. The MSD plots of the COM of the alpha carbon atoms of the protein show that in the WT-0%PA system, where the protein does not interact with the membrane, the protein diffuses almost an order of magnitude faster (S2 Fig). The mobility of the proteins, which interact with the membrane is similar for all systems and is very close to the mobility of the PAs and show a diffusive behavior (S2 Fig). This observation indicates a strong dynamic correlation of protein COM and PA dynamics.

2.2 Importance of amino acids in protein-membrane binding

Next we studied the protein-membrane binding on the level of single amino acids in the polybasic region of LKB1. To characterize these properties in the long-time stationary regime, we averaged the fraction of bound PAs during the last 500 ns of the simulation (Fig 5A-D). One can clearly identify three groups of positively charged residues of the protein, i.e., KKK, KRR and KK, which display a particularly strong attraction of PAs. The respective time-dependencies (summed over each group) are additionally displayed in S3 Fig. As already known, during the simulation time no complete convergence of the WT-20%PA binding is reached so that actual number of contacts in the long-time limit is expected to be higher.

The KRR group establishes the highest number of contacts with the PAs, which is likely due to the presence of arginine residues in this group. The other two groups show

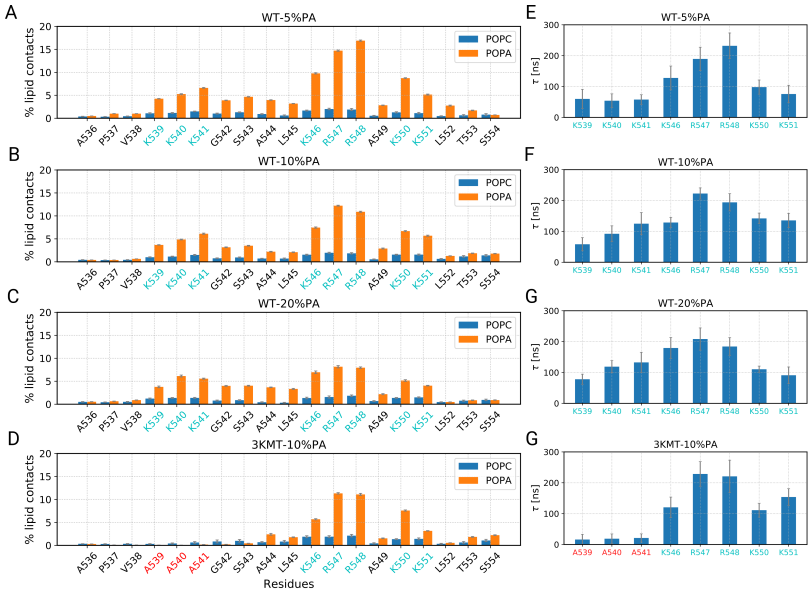

Fig 5. Interaction of different lipid types with the protein residues and the residence time of PAs. A-D) The average of the percentage of different lipid types interacting with all the protein residues over the last 500 ns of the simulation. E-H) The average residence time of PAs with the amino acids in the polybasic region of the protein. The residence times were calculated from the auto-correlation function of the time series of the number of contacts of PAs with the polar residues.

a somewhat smaller but still significant affinity to the membrane. As already discussed in the context of Fig 4, the fraction of bound PAs does not change much despite the enormous (factor of 4) variation of the PA concentration. Only for the KRR group the fraction of lipid contacts somewhat increases for smaller PA content. This suggests that there are specific PA-binding sites in this group.

As expected, the 3KMT-10%PA system shows a negligible number of contacts of the mutated residues with the PAs whereas the other groups show a similar behavior as the wildtype.

Moreover, it is also interesting to probe with how many PA lipids each polar residue interacts (S4 Fig). The results obviously depend on the amount of PAs in the system. For the WT-5%PA system, for instance, at most two PAs can bind to these residues (S4 FigA), whereas for the WT-10%PA system the arginine residues and K550 can bind also to 3 PA lipids at the same time (S4 FigB). For the WT-10%PA system, almost all the residues can bind to three PAs (S4 FigC), while for the 3KMT-10% system this is mainly the case only for the arginine residues (S4 FigD).

Additional information can be gained from the analysis of the residence times of an individual PA molecule at specific binding site, based on the auto-correlation function of the time series of the protein-lipid contacts (Fig 5E-H). Interestingly, in agreement with the structural properties, the second group of amino acids in the polybasic region, i.e., KRR, shows longer residence times, which is again likely due to the presence of arginine residues in this group. This highlights the expected correlation between high binding affinity and long residence times. For comparison we also calculated the residence time of PAs with the entire protein, which is around 350 ns, and thus, approximately only three times longer than the average residence time with the individual residues. This shows that there is a gradual exchange of the PAs, which interacts with the protein, highlighting a highly dynamic binding. At the same time it is interesting to compare

the MSD at 350 ns (which is approximately 60 nm^2) (S5 Fig) with the projected area of the protein on the membrane (which is approximately 93.6 nm^2 for the case of the WT-10%PA system). These values are relatively close to each other, which implies that a scenario where the bound PA diffuse together with the protein over distances much longer than the protein size can be excluded (S6 FigA). Instead, the protein-lipid binding has a restricted temporal-space behavior (S6 FigB).

3 Results: PA perspective

3.1 Agglomeration of PAs

Since the polybasic motif of LKB1 interacts mainly with PAs, this suggests that the protein can induce the agglomeration of PAs and as a result affect the lateral distribution of PAs. To probe this effect in more detail, we first calculated the radial distribution function (RDF or $g(r)$) of PAs along the xy-plane (Fig 6). To compare the effect of the protein-membrane interaction, we considered the MT-10%PA system as a control system since the protein does not interact with the membrane and no change in the behavior of PA should be observed. We always used the last 500 ns of the simulation to be sensitive to the stationary situation.

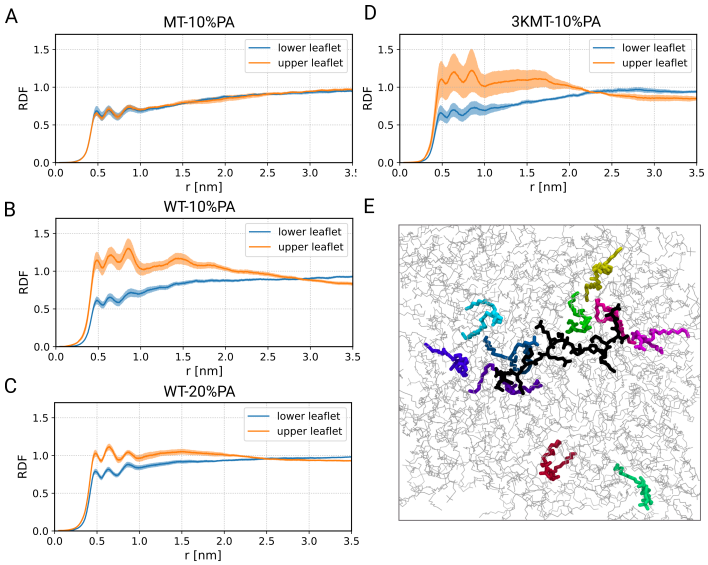

Fig 6. Protein-membrane interaction results in accumulation of PAs. (A-D) The RDF profile of PAs in the upper leaflet (the interacting leaflet) and the lower leaflet for the last 500 ns of the simulation for different systems. E) A snapshot of the protein-membrane system (WT-10%PA) from the top view is shown. The protein and the PAs in the interacting leaflet are shown respectively in black and colored licorice representation. The PC lipids are shown in grey lines.

Without the impact of the protein the PAss are strongly repelling each other for both leaflets (Fig 6A). This is a consequence of the mutual Coulomb repulsion. Remarkably, it gives rise to a radial distribution function $g(r) < 1$ for basically all distances. In contrast, in the presence of bound LKB1 (Fig 6B-D) one observes some agglomeration effects, i.e. $g(r) > 1$, in the upper leaflet (interacting leaflet), whereas the PA structure in the lower leaflet is basically unmodified. This is due to the fact that the protein tends to interact with PAs and, as a consequence, it induces their agglomeration. A typical realization can be found in Fig 6E.

Furthermore, in S7 Fig we plot the time evolution of the first peak of the RDF. As expected, the observed increase with time reflects the increase of binding PAs, as shown in Fig 4. Interestingly, for the MT-10%PA system the peak height decreases with time. Thus, it takes time to accomplish a configuration where the PAs efficiently repel themselves .

Next, we studied the number of PA molecules interacting with the polybasic motif of LKB1 for the cases of the WT and 3KMT-10%PA systems. From the last 500 ns of the simulation we estimated their average number μ_{sim} as well as their fluctuations, expressed by the standard deviation σ_{sim} of their distribution. To find an interpretation of the size of the fluctuations, we compared these values with the expectation when assuming a binomial distribution, i.e. $\sigma_{sim}^{binomial} = \sqrt{p(1-p)/M}$, where p is the probability that PAs interact with the protein and M is the number of PAs. The values for μ_{sim} and $\sigma_{sim}/\sigma_{sim}^{binomial}$ are listed in Table 3. Interestingly, the actual fluctuations are somewhat smaller than the predictions of the binomial distribution. This effect is particularly pronounced for membranes with a higher PA concentration.

Table 3. Fluctuations of interacting PAs: Comparison of simulations with the predictions of the fluctuation model.

system	r	μ_{sim}	$\sigma_{sim}/\sigma_{sim}^{binomial}$	μ_{model}	$\sigma_{model}/\sigma_{model}^{binomial}$
WT-5%PA	7.2	38.5	0.90	38.5	0.90
WT-10%PA	7.4	34.5	0.81	32.0	0.82
WT-20%PA	7.7	28.6	0.64	24.4	0.72
3KMT-10%PA	6.4	26.3	0.78	29.1	0.78

To obtain a mechanistic understanding of the protein-membrane binding, we formulated a minimal model, incorporating the following key effects. (1) Without binding and repulsion, the distribution is a binomial distribution. The probability r of a lipid to be bound can be estimated from the MD simulations when analysing whether a randomly placed lipid is counted as a bound or an unbound lipid. The values for r slightly depend on the chosen protein and PA composition and are listed in Table 3. (2) A binding PA molecule experiences a binding energy E_1 (here expressed relative to temperature). (3) There exists a maximal number n_{max} of lipids. For reasons of simplicity this value is chosen as the number of polar amino acids in the polybasic region, i.e. $n_{max} = 8$ for the WT and $n_{max} = 5$ for 3KMT. (4) Bound lipids repel each other due to Coulomb interaction. If at a given time one has n bound PAs, this can be expressed (again relative to temperature) as $E_2(n-1)^2$ where the quadratic dependence corresponds to a mean-field approximation. We denote the resulting model as *fluctuation model*.

The probability to have n bound PAs is proportional to $\binom{M}{n}[r/(1-r)]^n \exp[E_1 \cdot n - E_2 \cdot (n-1)^2]$ if $n \leq n_{max}$ and 0 otherwise. From this distribution the different moments of the distribution of bound lipids can be easily calculated. The two adjustable parameters E_1 and E_2 can be determined from reconstructing the first and second moment for WT-5%PA, yielding $E_1 = 2.33$ and $E_2 = 0.12$. Indeed, for $E_2 = 0$ there are no deviations from the binomial distribution because the upper limit $n_{max} = 8$ does not matter for $M = 5$. Thus, both the repulsion of lipids as well as the presence of a maximum number of bound lipids reduces the fluctuations as compared to the binomial distribution. For the estimation of E_1 one can obtain an analytical approximation from the relation $r/(1-r)\exp(E_1) = \mu/(1-\mu)$, which strictly holds for $E_2 = 0$. For WT-5%PA this yields $E_1 = 2.08$ which is close to the actual fitted value of 2.33.

The predictions of the fluctuation model for the other three cases are shown in Table 3 and the two adjustable energy parameters, representing attraction and repulsion

effects, as obtained from the WT-5%PA system. One can indeed find a very good agreement between the actual numerical data and these predictions for all three cases. Thus, one may conclude that to a reasonable approximation the binding properties can be related to this simple fluctuation model. Two key conclusions can be drawn. First, the model analysis shows that both due to the stronger repulsion effects upon crowding as well as due to the presence of a maximum number of binding sites, the fluctuations are reduced as compared to the binomial distribution, as also seen for the simulation data., indicating the importance of these effects. Second, the description of the observed fluctuations of a relatively small system via the fluctuation model allows for a straightforward estimation of the relevant energy parameters, expressing the typical binding (free) energy as well as the repulsive energy.

The agglomeration of PAs can be additionally observed in the density maps of PAs, considering the protein at the center of the density map and looking at the position of lipids around it (Fig 7A). It is clearly observed that for the lower leaflet the lipids are distributed homogeneously (Fig 7A right), whereas for the upper leaflet a considerable accumulation of PA is obvious (Fig 7A left).

The interaction of the polybasic motif of LKB1 with the membrane can also affect the membrane properties. Here we study the height profiles of the lipids' headgroups and the resulting thickness of the membrane. We calculated the height profiles again by placing the protein at the center of the membrane and calculating the height profiles of the P atoms of the PC lipids (Fig 7B). Interestingly, we see that the surface of the membrane close to the position of the protein is around 2 $\AA$ deeper than the other parts, meaning that the protein is somehow absorbed by the membrane. This is likely associated with additional structural changes in the lipids structure, i.e., the order parameter of the lipid chains, which adopts lower values for the lipids in the vicinity of the protein (Fig 7C).

Discussion

In this work, we probed the interaction of the C-terminus of LKB1, which adopts a disordered structure with membranes containing different concentrations of PA. To the best of our knowledge, the computational studies of the interaction of IDPs with anionic membranes has not been reported so far. Interestingly, we observed that PA is imperative for the protein-membrane binding, which is in agreement with cell culture experiments using GFP-LKB1 variants. These observations are similar to the RIT1 protein, which is also localized to the PM and lacks the C-terminal prenylation, which helps many other subfamily members to adhere to cellular membranes. The MD simulations of the C-terminus of tRIT1, which is also unstructured, revealed a dependency of the membrane interactions on the lipid composition in membranes containg POPC/POPS [10].

We additionally showed that mutation of the first three Lysines within the polybasic motif (the3KMT) did not prevent the protein-membrane binding, which is again in line with the corresponding cell culture experiments. Moreover, the effect of PAs was found to be more significant than the polybasic region since the mutation of all the amino acids in this region showed comparatively more attractive interaction with the membrane containing 10% PA than the WT protein with the membranes without PA . Furthermore, we showed that the middle group of residues in the polybasic region plays a more important role than the adjacent groups, which might be associated to the presence arginine residues, as this amino acid has been shown to attract phosphate and establish extensive H-bonding [36]. Consistently, higher residence times of PA molecules were observed with arginine residues compared to lysine residues.

Moreover, we observed that as a result of the interaction of LKB1 with PA within

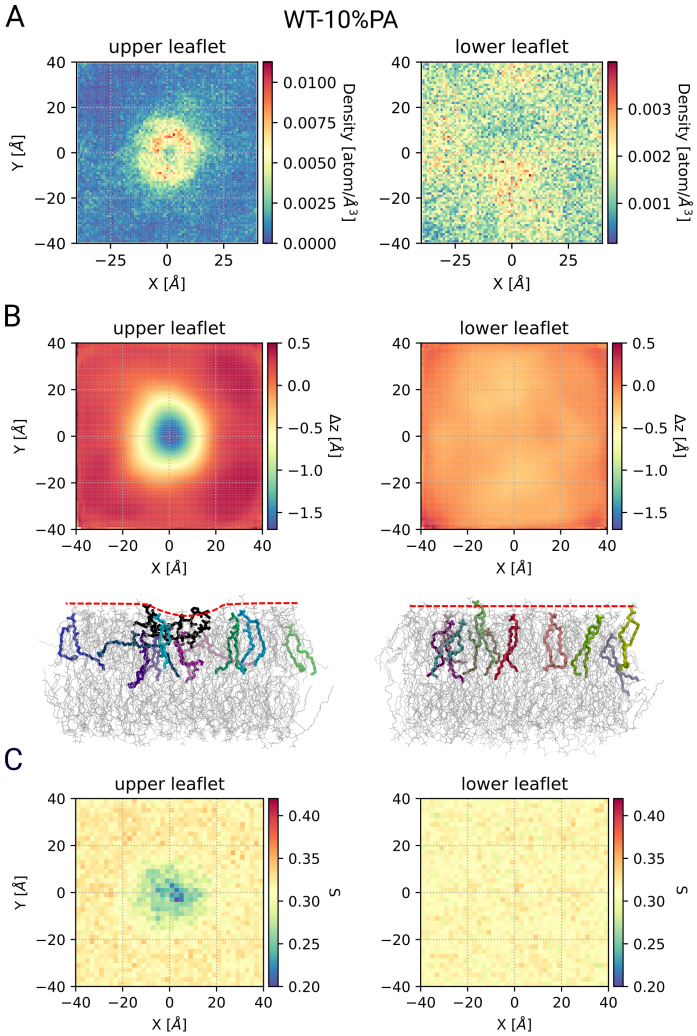

Fig 7. Density of PA and membrane properties. A) Density maps of PAs for the WT-10%PA system when considering the protein at the center of the membrane. Therefore, the density maps were calculated by changing the coordinates in a way that the protein is kept always at the center of the membrane along the xy-plane. B) The height profiles of the upper and lower leaflets for the WT-10%PA system, when considering the protein always at the center of the membrane, are shown. Only the position of P atoms of PC lipids was used for these calculations. Subsequently, for each leaflet the average COM of the P atoms in the respective leaflet was subtracted from the height positions along the membrane normal. The snapshots of the protein-membrane system for the interacting (left) and non-interacting (right) are shown. The approximate surface of the membrane is shown by a red dashed line. The protein and PA molecules in one leaflet are shown respectively in black and colored licorice representation. The PC lipids are shown as grey lines. C) The order parameter of PA and PC lipid chains for the WT-10%PA system again when considering the protein at the center of the membrane.

the membrane the structural properties of the protein are modified in a typical time-dependent manner. Generally, membrane-bound protein was less flexible on the membrane compared to the in solution state. As a result of the dynamic movement of

the protein and the lipids and their mutual interaction, the compactness of the protein along the membrane normal and the membrane plane is modified throughout the simulation. First, it acquires a prolate form; this might be because at the beginning the protein tries to find an optimal interaction with the PA and once it is equilibrated on the membrane, its flatness decreases. These results are reminiscent of the general behavior of IDPs, i.e., their slow relaxation, associated with their large conformational entropy. In our case it required microsecond simulations to cover part of their conformational ensembles. In order to alleviate the sampling limitations, we used different samples for each system, starting from different protein structures. It should also be noted that the force fields for IDPs have improved noticeably [23, 37–39], particularly due to the dispersion-corrected water models [40], which have resulted in better solvation, and therefore, more realistic simulations. Nonetheless, the accuracy of the simulation results, assessed by the comparison with experimenters, was revealed to depend on the specific IDP, the used force field, and the configurational sampling [23, 38, 39, 41–44].

Due to the protein-membrane interaction, the arrangement of PA molecules in the membrane changed and showed a dynamic clustering in the proximity of the protein only in the interacting leaflet. Thus, as the protein moves on the membrane, it is binding to PA and this attraction along with its movement on the membrane induces clustering of the PA and fluctuations in the number of interacting PAs. Furthermore, by describing the observed fluctuations via our fluctuation model, we could obtain a straightforward estimation of energy parameters, one of which expresses a typical binding energy with the value of 2.33 k_BT. This value is characteristic for the binding free energy of proteins to charged lipids such as PS and PIP2 [45–47]. In the work of Larsen et al, for instance, the free energy of binding for individual PIP2 ranges from 1.61 to 8.47 k_BT, depending on the side of the interacting protein [48]. However, as shown in the this work, the binding energy for PIP2 is considerably higher than PS. In the work of Yamamoto et al., it is observed that the binding energy decreases with the increase in the number of lipids in the membrane; it is, however, not clear how many lipids interact with the protein in each case [48]. One should also keep in mind that the free energy of binding depends also on the number and nature of the polar residues in the protein structure. Furthermore, the protein-membrane interaction had also an effect on membrane properties, namely, the height profiles of lipids, and therefore, the membrane thickness, and showed some sort of adsorption of the protein onto the membrane. This becomes also clear in the density profiles of proteins along the membrane normal (Figure 1G). This adsorption can be associated to the formation of PA-rich domains in the vicinity of the protein, and in turn, the structural changes of the interacting lipids in the form of order parameter of the lipids' acyl chains. The clustering of anionic lipids and the change in membrane properties has been also observed in the MD simulations of strong polycations with a POPC/POPS membrane [49]. A similar clustering behavior has been reported in the case of polyethylenimines with a POPC/DOPA

Conclusion

In summary, we revealed that the polybasic motif of LKB1 can establish stable, albeit highly dynamic, binding with membranes with low amounts of PA. This suggests that farnesylation of LKB1 is not specifically required for stable association of LKB1 with membranes, which has been supported by in vivo experiments (Dogliotti et al. [8, 35], Borkowsky at el., in press). Furthermore, the LKB1-membrane interaction revealed interesting mutual effects of the protein and anionic lipids, such as proteins' structural modifications and agglomeration of PAs, providing microscopic insights into the interaction of LKB1 and other IDPs with membranes containing anionic lipids.

Supporting information

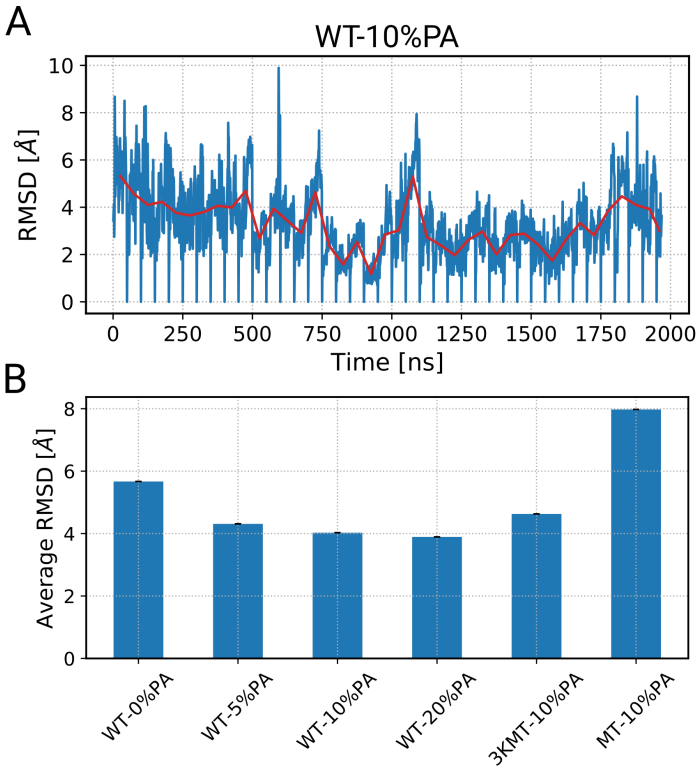

S1 Fig. RMSD of the protein. A) RMSD of the protein backbone in slices of 50ns (taking the structure at the beginning of each slice as a reference structure. The running average for each block is shown in red line. B) The average RMSD of the protein backbone for each system. The averaging is done over the RMSD values of all slices considering the data of the second half each slice.

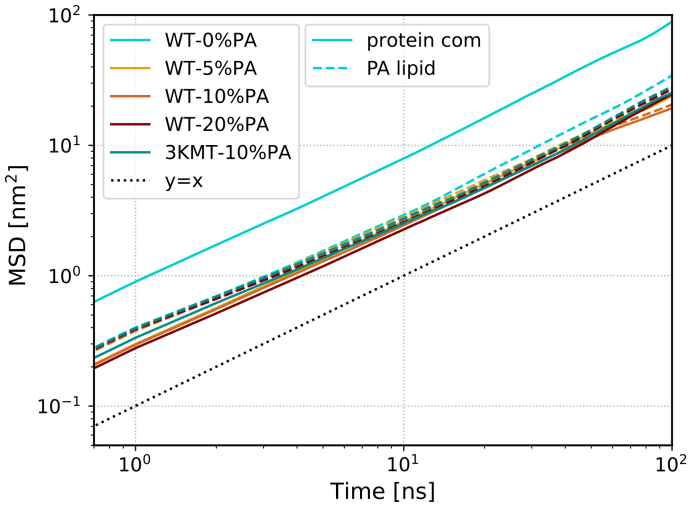

S2 Fig. Protein and lipids show similar dynamics. MSD of the COM of the protein as well as P atoms of PAs are represented for different systems.

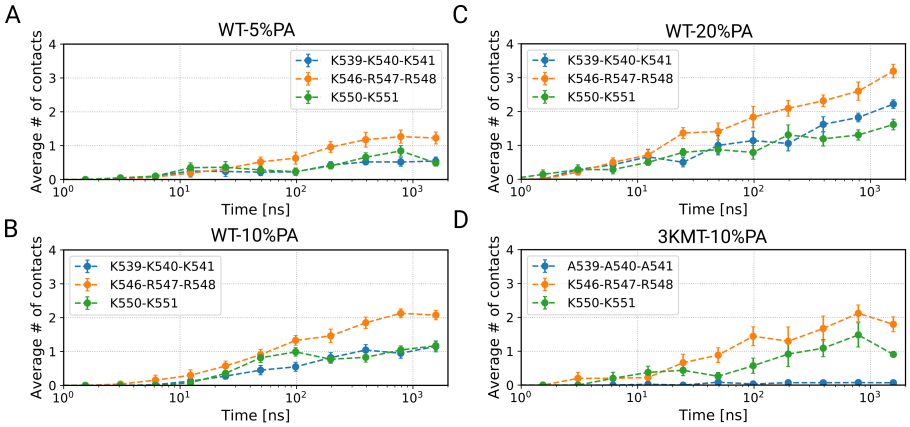

S3 Fig. Interaction of PA with different blocks of residues in the polybasic region. The average number of PA lipids bound to the three groups of positively-charged residues throughout the simulation time.

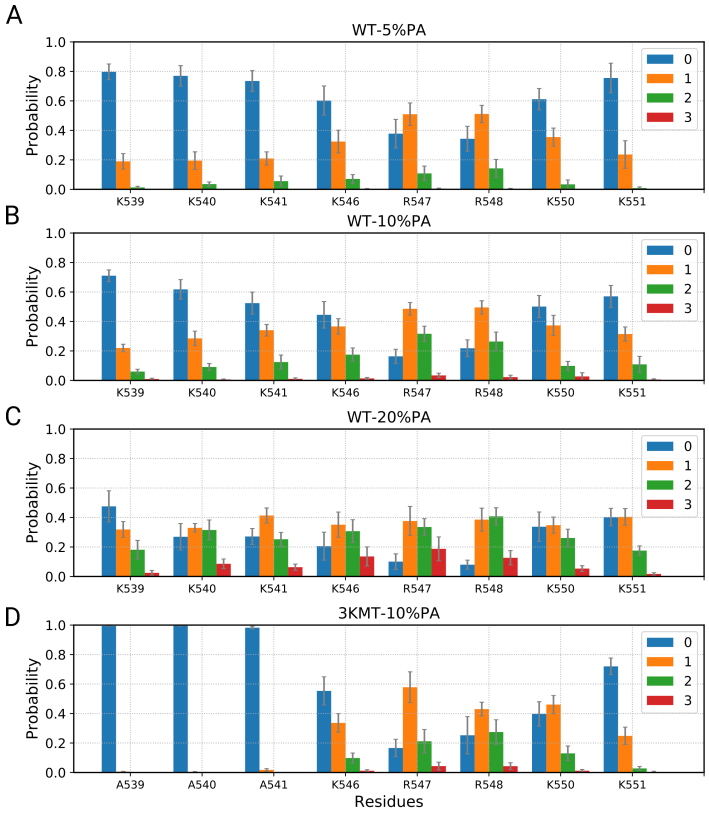

S4 Fig. Number of PA contacts with each protein residue. The probability of the average number of PA lipid contacts interacting with each residue in the poly-basic region.

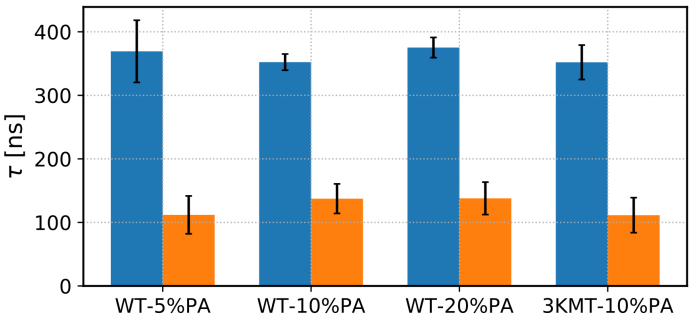

S5 Fig. Residence time of PA with the protein. The average residence time of PA molecules with the whole protein (blue) and the polar residues in the poly-basic region (orange). The residence times were calculated from the auto-correlation function of the time series of the number of the number of contacts of PAs with the whole protein and the polar residues.

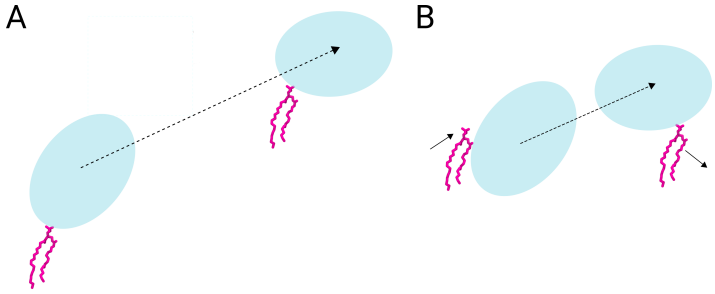

S6 Fig. Two scenarios for the protein-lipid binding. Schematic representation of two different scenarios concerning the interaction of a PA molecule with the protein. A) A scenario in which an interacting PA remains bonded to the protein when the protein moves larges distances is shown. B) A scenario in which a PA molecule interacts temporarily with the protein, when the protein traverse a distance in the order of its area is represented. The PA molecule is shown in licorice representation, whereas the protein is depicted via ellipses. The movement of the protein is shown by a dashed line arrow.

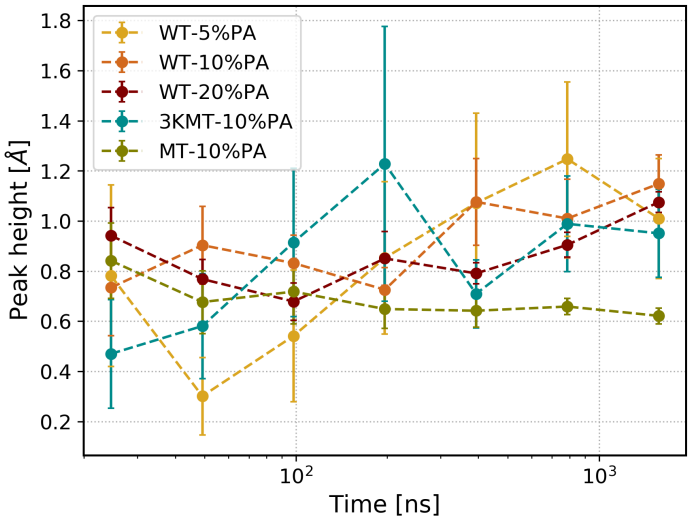

S7 Fig. Evolution of the RDF peak during the simulation time. The average of the height of the first peak in the RDF profiles in the course of the simulation.

Acknowledgments

The authors thank the high performance computer resources at University of Muenster (Palma) and the financial support by the German Science Foundation (DFG, projects CRC1348-A01 and CRC1348-A05) and the Interdisciplinary Centre for Clinical Research (IZKF) Münster (Kr-A-031.21).

References

1. Lizcano JM, Göransson O, Toth R, Deak M, Morrice NA, Boudeau J, et al. LKB1 is a master kinase that activates 13 kinases of the AMPK subfamily, including MARK/PAR-1. The EMBO Journal. 2004;23(4):833–843. doi:https://doi.org/10.1038/sj.emboj.7600110.

2. Vaahtomeri K, Mäkelä TP. Molecular mechanisms of tumor suppression by LKB1. FEBS Letters. 2011;585(7):944–951. doi:https://doi.org/10.1016/j.febslet.2010.12.034.

3. Nakano A, Takashima S. LKB1 and AMP-activated protein kinase: regulators of cell polarity. Genes to Cells. 2012;17(9):737–747. doi:https://doi.org/10.1111/j.1365-2443.2012.01629.x.

4. Boudeau J, Baas AF, Deak M, Morrice NA, Kieloch A, Schutkowski M, et al. MO25α/β interact with STRADα/β enhancing their ability to bind, activate and localize LKB1 in the cytoplasm. The EMBO Journal. 2003;22(19):5102–5114. doi:https://doi.org/10.1093/emboj/cdg490.

5. Dorfman J, Macara IG. STRADα Regulates LKB1 Localization by Blocking Access to Importin-α, and by Association with Crm1 and Exportin-7. Molecular Biology of the Cell. 2008;19(4):1614–1626. doi:10.1091/mbc.e07-05-0454.

6. Sapkota GP, Kieloch A, Lizcano JM, Lain S, Arthur JSC, Williams MR, et al. Phosphorylation of the Protein Kinase Mutated in Peutz-Jeghers Cancer Syndrome, LKB1/STK11, at Ser431 by p90RSK and cAMP-dependent Protein Kinase, but Not Its Farnesylation at Cys433, Is Essential for LKB1 to Suppress Cell Growth*. Journal of Biological Chemistry. 2001;276(22):19469–19482. doi:https://doi.org/10.1074/jbc.M009953200.

7. Houde V, Ritorto M, Gourlay R, Varghese J, Davies P, Shpiro N, et al. Investigation of LKB1 Ser431 phosphorylation and Cys433 farnesylation using mouse knockin analysis reveals an unexpected role of prenylation in regulating AMPK activity. Biochemical Journal. 2014;458(1):41–56. doi:10.1042/BJ20131324.

8. Dogliotti G, Kullmann L, Dhumale P, Thiele C, Panichkina O, Mendl G, et al. Membrane-binding and activation of LKB1 by phosphatidic acid is essential for development and tumour suppression. Nature Communications. 2017;8(1):15747. doi:10.1038/ncomms15747.

9. Stace CL, Ktistakis NT. Phosphatidic acid- and phosphatidylserine-binding proteins. Biochimica et Biophysica Acta (BBA) - Molecular and Cell Biology of Lipids. 2006;1761(8):913–926. doi:https://doi.org/10.1016/j.bbalip.2006.03.006.

10. Migliori AD, Patel LA, Neale C. The RIT1 C-terminus associates with lipid bilayers via charge complementarity. Computational Biology and Chemistry. 2021;91:107437. doi:https://doi.org/10.1016/j.compbiolchem.2021.107437.

11. Kullmann L, Krahn MP. Controlling the master—upstream regulation of the tumor suppressor LKB1. Oncogene. 2018;37(23):3045–3057. doi:10.1038/s41388-018-0145-z.

12. Krahn MP, Klopfenstein DR, Fischer N, Wodarz A. Membrane Targeting of Bazooka/PAR-3 Is Mediated by Direct Binding to Phosphoinositide Lipids. Current Biology. 2010;20(7):636–642. doi:https://doi.org/10.1016/j.cub.2010.01.065.

13. Dong W, Zhang X, Liu W, Chen Yj, Huang J, Austin E, et al. A conserved polybasic domain mediates plasma membrane targeting of Lgl and its regulation by hypoxia. Journal of Cell Biology. 2015;211(2):273–286. doi:10.1083/jcb.201503067.

14. Waterhouse A, Bertoni M, Bienert S, Studer G, Tauriello G, Gumienny R, et al. SWISS-MODEL: homology modelling of protein structures and complexes. Nucleic acids research. 2018;46(W1):W296–W303. doi:10.1093/nar/gky427.

15. Bienert S, Waterhouse A, de Beer TAP, Tauriello G, Studer G, Bordoli L, et al. The SWISS-MODEL Repository-new features and functionality. Nucleic acids research. 2017;45(D1):D313–D319. doi:10.1093/nar/gkw1132.

16. Guex N, Peitsch MC, Schwede T. Automated comparative protein structure modeling with SWISS-MODEL and Swiss-PdbViewer: a historical perspective. Electrophoresis. 2009;30 Suppl 1:S162–73. doi:10.1002/elps.200900140.

17. Jo S, Kim T, Iyer VG, Im W. CHARMM-GUI: A web-based graphical user interface for CHARMM. Journal of Computational Chemistry. 2008;29(11):1859–1865. doi:10.1002/jcc.20945.

18. Antila H, Buslaev P, Favela-Rosales F, M Ferreira T, Gushchin I, Javanainen M, et al. Headgroup Structure and Cation Binding in Phosphatidylserine Lipid Bilayers. The Journal of Physical Chemistry B. 2019;123(43):9066–9079. doi:10.1021/acs.jpcb.9b06091.

19. Catte A, Girych M, Javanainen M, Loison C, Melcr J, Miettinen MS, et al. Molecular electrometer and binding of cations to phospholipid bilayers. Physical Chemistry Chemical Physics. 2016;18(47):32560–32569. doi:10.1039/C6CP04883H.

20. Lindahl E, Hess B, van der Spoel D. GROMACS 3.0: a package for molecular simulation and trajectory analysis. Molecular modeling annual. 2001;7(8):306–317. doi:10.1007/s008940100045.

21. Van Der Spoel D, Lindahl E, Hess B, Groenhof G, Mark AE, Berendsen HJC. GROMACS: Fast, flexible, and free. Journal of Computational Chemistry. 2005;26(16):1701–1718. doi:10.1002/jcc.20291.

22. B Klauda J, M Venable R, Alfredo Freites J, W O'Connor J, J Tobias D, Mondragon-Ramirez C, et al. Update of the CHARMM All-Atom Additive Force Field for Lipids: Validation on Six Lipid Types. The Journal of Physical Chemistry B. 2010;114(23):7830–7843. doi:10.1021/jp101759q.

23. Huang J, Rauscher S, Nawrocki G, Ran T, Feig M, de Groot BL, et al. CHARMM36m: an improved force field for folded and intrinsically disordered proteins. Nature Methods. 2017;14(1):71–73. doi:10.1038/nmeth.4067.

24. Jorgensen WL, Chandrasekhar J, Madura JD, Impey RW, Klein ML. Comparison of simple potential functions for simulating liquid water. The Journal of Chemical Physics. 1983;79(2):926–935. doi:10.1063/1.445869.

25. Essmann U, Perera L, Berkowitz ML, Darden T, Lee H, Pedersen LG. A smooth particle mesh Ewald method. The Journal of Chemical Physics. 1995;103(19):8577–8593. doi:10.1063/1.470117.

26. Berendsen HJC, Postma JPM, van Gunsteren WF, DiNola A, Haak JR. Molecular dynamics with coupling to an external bath. The Journal of Chemical Physics. 1984;81(8):3684–3690. doi:10.1063/1.448118.

27. Parrinello M, Rahman A. Polymorphic transitions in single crystals: A new molecular dynamics method. Journal of Applied Physics. 1981;52(12):7182–7190. doi:10.1063/1.328693.

28. Nosé S. A unified formulation of the constant temperature molecular dynamics methods. The Journal of Chemical Physics. 1984;81(1):511–519. doi:10.1063/1.447334.

29. Hoover WG. Canonical dynamics: Equilibrium phase-space distributions. Phys Rev A. 1985;31(3):1695–1697. doi:10.1103/PhysRevA.31.1695.

30. Hess B, Bekker H, Berendsen HJC, Fraaije JGEM. LINCS: A linear constraint solver for molecular simulations. Journal of Computational Chemistry. 1997;18(12):1463–1472. doi:10.1002/(SICI)1096-987X(199709)18:12¡1463::AID-JCC4¿3.0.CO;2-H.

31. Michaud-Agrawal N, Denning EJ, Woolf TB, Beckstein O. MDAnalysis: A Toolkit for the Analysis of Molecular Dynamics Simulations. Journal of computational chemistry. 2011;32(10):2319–2327. doi:10.1002/jcc.21787.

32. Gowers RJ, Linke M, Barnoud J, Reddy TJE, Melo MN, Seyler SL, et al. MDAnalysis : A Python Package for the Rapid Analysis of Molecular Dynamics Simulations MDAnalysis. 2016;(Scipy):98–105.

33. Humphrey W, Dalke A, Schulten K. VMD: Visual molecular dynamics. Journal of Molecular Graphics. 1996;14(1):33–38. doi:http://dx.doi.org/10.1016/0263-7855(96)00018-5.

34. Róg T, Pasenkiewicz-Gierula M, Vattulainen I, Karttunen M. Ordering effects of cholesterol and its analogues. Biochimica et Biophysica Acta (BBA) - Biomembranes. 2009;1788(1):97–121. doi:https://doi.org/10.1016/j.bbamem.2008.08.022.

35. Borkowsky S, Gass M, Alavizargar A, Hanewinkel J, Hallstein I, Nedvetsky P, et al.. Phosphorylation of LKB1 by PDK1 Inhibits Cell Proliferation and Organ Growth by Decreased Activation of AMPK; 2023.

36. Li L, Vorobyov I, W Allen T. The Different Interactions of Lysine and Arginine Side Chains with Lipid Membranes. The Journal of Physical Chemistry B. 2013;117(40):11906–11920. doi:10.1021/jp405418y.

37. Rauscher S, Gapsys V, J Gajda M, Zweckstetter M, L de Groot B, Grubmüller H. Structural Ensembles of Intrinsically Disordered Proteins Depend Strongly on Force Field: A Comparison to Experiment. Journal of Chemical Theory and Computation. 2015;11(11):5513–5524. doi:10.1021/acs.jctc.5b00736.

38. Robustelli P, Piana S, Shaw DE. Developing a molecular dynamics force field for both folded and disordered protein states. Proceedings of the National Academy of Sciences. 2018;115(21):E4758–E4766. doi:10.1073/pnas.1800690115.

39. Liu H, Song D, Lu H, Luo R, Chen HF. Intrinsically disordered protein-specific force field CHARMM36IDPSFF. Chemical biology & drug design. 2018;92(4):1722–1735. doi:10.1111/cbdd.13342.

40. Piana S, G Donchev A, Robustelli P, E Shaw D. Water Dispersion Interactions Strongly Influence Simulated Structural Properties of Disordered Protein States. The Journal of Physical Chemistry B. 2015;119(16):5113–5123. doi:10.1021/jp508971m.

41. Henriques J, Arleth L, Lindorff-Larsen K, Skepö M. On the Calculation of SAXS Profiles of Folded and Intrinsically Disordered Proteins from Computer Simulations. Journal of molecular biology. 2018;430(16):2521–2539. doi:10.1016/j.jmb.2018.03.002.

42. Henriques J, Cragnell C, Skepö M. Molecular Dynamics Simulations of Intrinsically Disordered Proteins: Force Field Evaluation and Comparison with Experiment. Journal of Chemical Theory and Computation. 2015;11(7):3420–3431. doi:10.1021/ct501178z.

43. Henriques J, Skepö M. Molecular Dynamics Simulations of Intrinsically Disordered Proteins: On the Accuracy of the TIP4P-D Water Model and the Representativeness of Protein Disorder Models. Journal of Chemical Theory and Computation. 2016;12(7):3407–3415. doi:10.1021/acs.jctc.6b00429.

44. Koder Hamid M, Månsson LK, Meklesh V, Persson P, Skepö M. Molecular dynamics simulations of the adsorption of an intrinsically disordered protein: Force field and water model evaluation in comparison with experiments. Frontiers in molecular biosciences. 2022;9:958175. doi:10.3389/fmolb.2022.958175.

45. Yamamoto E, Domański J, Naughton FB, Best RB, Kalli AC, Stansfeld PJ, et al. Multiple lipid binding sites determine the affinity of PH domains for phosphoinositide-containing membranes. Science Advances. 2023;6(8):eaay5736. doi:10.1126/sciadv.aay5736.

46. Larsen AH, John LH, Sansom MSP, Corey RA. Specific interactions of peripheral membrane proteins with lipids: what can molecular simulations show us? Bioscience Reports. 2022;42.

47. Zhang X, Zhang W, González-Cobos JC, Jardin I, Romanin C, Matrougui K, et al. Complex role of STIM1 in the activation of store-independent Orai1/3 channels. The Journal of general physiology. 2014;143(3):345–359. doi:10.1085/jgp.201311084.

48. Larsen AH, Sansom MSP. Binding of Ca2+-independent C2 domains to lipid membranes: A multi-scale molecular dynamics study. Structure. 2021;29(10):1200–1213.e2. doi:https://doi.org/10.1016/j.str.2021.05.011.

49. Kopec W, Żak A, Jamróz D, Nakahata R, Yusa Si, Gapsys V, et al. Polycation–Anionic Lipid Membrane Interactions. Langmuir. 2020;36(42):12435–12450. doi:10.1021/acs.langmuir.0c01062.